

Myelin Water Fraction Imaging Reveals Hemispheric Asymmetries in Human White Matter That Are Associated with Genetic Variation in PLP1

Sebastian Ocklenburg, Catrona Anderson, Wanda M. Gerding, Christoph Fraenz, Caroline Schlüter, Patrick Friedrich, Maximilian Raane, et

Molecular Neurobiology

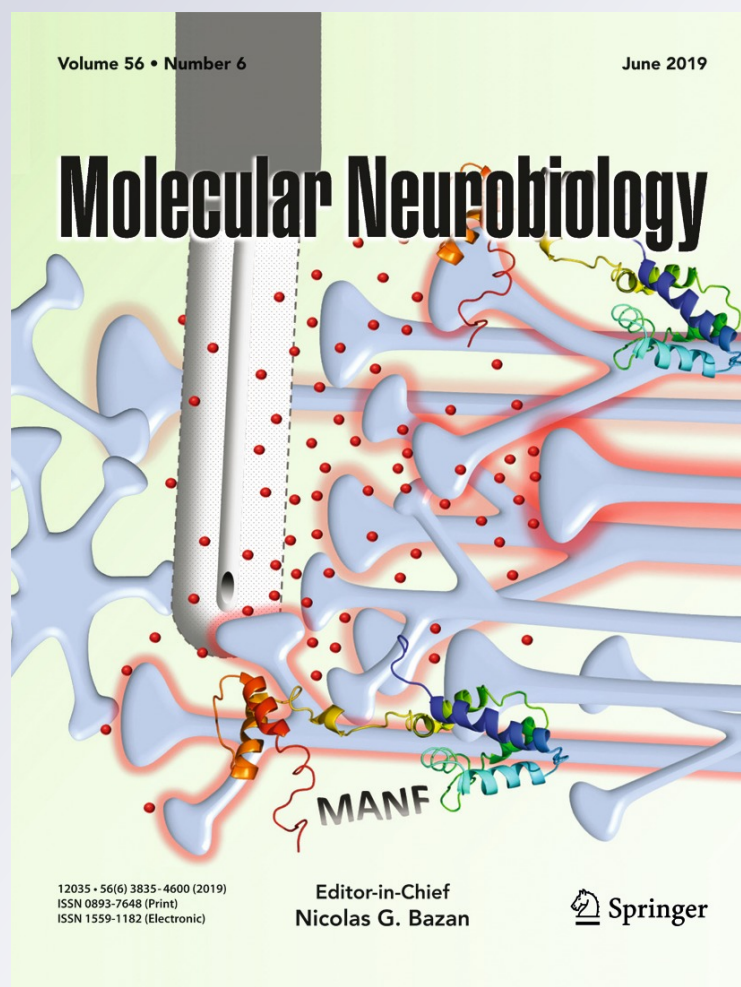
ISSN 0893-7648

Volume 56

Number 6

Mol Neurobiol (2019) 56:3999-4012

DOI 10.1007/s12035-018-1351-y



Your article is protected by copyright and all rights are held exclusively by Springer Science+Business Media, LLC, part of Springer Nature. This e-offprint is for personal use only and shall not be self-archived in electronic repositories. If you wish to self-archive your article, please use the accepted manuscript version for posting on your own website. You may further deposit the accepted manuscript version in any repository, provided it is only made publicly available 12 months after official publication or later and provided acknowledgement is given to the original source of publication and a link is inserted to the published article on Springer's website. The link must be accompanied by the following text: "The final publication is available at link.springer.com".



Myelin Water Fraction Imaging Reveals Hemispheric Asymmetries in Human White Matter That Are Associated with Genetic Variation in *PLP1*

Sebastian Ocklenburg¹ · Catrona Anderson^{1,2} · Wanda M. Gerding³ · Christoph Fraenz¹ · Caroline Schlüter¹ · Patrick Friedrich¹ · Maximilian Raane⁴ · Burkhard Mädler⁵ · Lara Schlaffke⁶ · Larissa Arning³ · Jörg T. Epplen^{3,4} · Onur Güntürkün¹ · Christian Beste⁷ · Erhan Genç¹

Received: 13 July 2018 / Accepted: 13 September 2018 / Published online: 21 September 2018
© Springer Science+Business Media, LLC, part of Springer Nature 2018

Abstract

Myelination of axons in the central nervous system is critical for human cognition and behavior. The predominant protein in myelin is proteolipid protein—making *PLP1*, the gene that encodes for proteolipid protein, one of the primary candidate genes for white matter structure in the human brain. Here, we investigated the relation of genetic variation within *PLP1* and white matter microstructure as assessed with myelin water fraction imaging, a neuroimaging technique that has the advantage over conventional diffusion tensor imaging in that it allows for a more direct assessment of myelin content. We observed significant asymmetries in myelin water fraction that were strongest and rightward in the parietal lobe. Importantly, these parietal myelin water fraction asymmetries were associated with genetic variation in *PLP1*. These findings support the assumption that genetic variation in *PLP1* affects white matter myelination in the healthy human brain.

Keywords White matter · Myelin · Myelin water fraction · Multi-exponential T2 relaxation · 3D multi-echo gradient spin echo (3D ME-GRASE) · Proteolipid protein · *PLP1* · Hemispheric asymmetries · Laterality · Brain

Sebastian Ocklenburg, Catrona Anderson and Wanda M. Gerding contributed equally to this work.

✉ Sebastian Ocklenburg
Sebastian.ocklenburg@rub.de

- ¹ Institute of Cognitive Neuroscience, Biopsychology, Department of Psychology, Ruhr University Bochum, Bochum, Germany
- ² Department of Psychology, University of Otago, Dunedin, New Zealand
- ³ Department of Human Genetics, Ruhr University Bochum, Bochum, Germany
- ⁴ Faculty of Health, ZBAF, University of Witten/Herdecke, Witten, Germany
- ⁵ Philips GmbH, Hamburg, Germany
- ⁶ Department of Neurology, BG-University Hospital Bergmannsheil, Ruhr University Bochum, Bochum, Germany
- ⁷ Cognitive Neurophysiology, Department of Child and Adolescent Psychiatry, Faculty of Medicine, TU Dresden, Dresden, Germany

Introduction

White matter is one of the two main components of the human cerebral cortex, making an understanding of its genetic determinants of pivotal interest for neuroscience [1]. White matter is mainly comprised of axons that are ensheathed by myelin in order to electrically insulate them and enhance the conduction speed of neuronal information by 10 to 100 times [2]. Myelin is therefore critical for human cognition and behavior, as conduction speed is an essential factor in coordinating complex cognition and motor behavior in order to interact with the environment [3, 4]. The predominant protein in myelin is proteolipid protein, which constitutes around 50% of myelin protein mass [5–7]. Proteolipid protein maintains the extracellular spacing of compact myelin by electrostatic interactions with myelin lipids [7]. It has been implicated in oligodendrocyte development, the formation of the intraperiod line of myelin, compaction of myelin, oligodendrocyte-axon interactions, wrapping of the axon, and axonal survival [8–12]. This makes *PLP1*, the gene that encodes for proteolipid protein, one of the primary candidate genes for white matter structure

[13]. *PLP1* is located at Xq22.2 and shows tissue-specific expression in the brain [14]. Mutations in *PLP1* can lead to rare X-linked myelination disorders like Pelizaeus-Merzbacher disease or spastic paraplegia type 2 [15].

PLP1 has been linked to white matter structure in the vertebrate brain. For example, Ruest et al. [16] performed high-resolution diffusion tensor imaging (DTI) of fixed brains obtained from mice transgenic for *Plp1*. Fractional anisotropy (FA) data, as well as axial and radial diffusivity data, were analyzed. Moreover, tract-based spatial statistics (TBSS), a method to assess whole-brain voxel differences in white matter [17], was used, as well as a region of interest (ROI) approach using the anterior commissure, corpus callosum, and hippocampal fimbria. For the whole-brain analyses, the authors found that the *Plp1*-transgenic mice showed significantly lower FA than wild-type mice. The TBSS analysis also showed a widespread reduction of FA and an increase in water diffusion in *Plp1*-transgenic mouse brains compared with wild-type mice. These results were also supported by the ROI analyses. Overall, the results indicated significant changes in white matter microstructure in the *Plp1*-transgenic mice. Widespread changes in white matter microstructure have also been reported in human patients with Pelizaeus-Merzbacher disease using DTI [18]. Other studies also reported tract-specific atrophies, e.g., for the corpus callosum [19] or the corticospinal tract [20] in these patients.

In addition, genetic variation in *PLP1* has also been linked to white matter function in the human brain. In a recent study using an interhemispheric integration task [21], it was shown that genetic variations in *PLP1* SNPs rs1126707 and rs521895 were related to interhemispheric integration, e.g., the integration of neuronal information between the left and right hemisphere via commissural white matter tracts to successfully complete a task [3]. In addition, it was shown that the same two SNPs were also associated with interindividual differences in dichotic listening and line bisection, two commonly used tasks to assess hemispheric asymmetries, e.g., functional differences between the two hemispheres [13]. As hemispheric asymmetries are thought to critically depend on white matter structure [22], these findings further support the idea that genetic variation in *PLP1* might be related to interindividual variations in white matter structure in the healthy human brain. However, the actual impact of genetic variation in *PLP1* on white matter microstructure in the healthy human brain is still completely unclear. Revealing this relationship would be a critical step in further understanding the relevance of *PLP1* for white matter organization in the human brain.

One of the most critical steps in investigating the neurogenetics of human white matter microstructure in vivo is to identify reliable neuroimaging protocols that specifically target myelin. Assessing the genetic determinants of white matter therefore critically depends on the signal-to-noise-ratio of the neuroimaging technique used to assess the

phenotype. If the generated images are influenced too much by factors other than white matter, existing associations might not be detected or non-existing associations might erroneously be assumed. The most commonly used imaging method to assess white matter microstructure is diffusion tensor imaging (DTI) [23]. DTI allows for both in vivo tractography of specific fiber tracts [24] and the quantification of white matter microstructure by determining the so-called fractional anisotropy (FA) [25, 26]. FA is seen as a measure of microstructural properties of white matter [27, 28] and is often assumed to reflect myelination. However, it has been shown that elevated degrees of diffusional anisotropies in highly organized fiber arrangements of compact white matter structures, such as the genu of the corpus callosum, do not necessarily correspond to elevated myelin content [29]. Instead, high FA more likely reflects the highly organized directionality of fiber bundles in these areas or strongly restricted diffusion in the interstitial space between the myelinated axons [29]. In general, recent research indicates that FA in white matter reflects not only myelin, but is determined by a multitude of influences, including axon diameter and packing density, axon permeability, and fiber geometry [28–31].

One non-invasive imaging method that may give a more accurate measure of myelin within white matter, and therefore might be a better neuroimaging method to use in *PLP1* studies than conventional DTI, is myelin water fraction (MWF) imaging [7, 29, 32–40]. MWF imaging is based on a MR sequence measuring the transversal relaxation time T_2 . In short, the water signal in the brain is constituted of three MR visible components at 3T: a long T_2 component (> 2 s) that is caused by cerebrospinal fluid (CSF), an intermediate T_2 component (70–100 ms) affiliated with the intracellular and extracellular water (IE), and a short T_2 component (10–30 ms) rising from water confined between the myelin bilayers [7]. Based on these values, the myelin water fraction can be determined for each voxel and can then be visualized in a myelin water fraction brain map.

MWF imaging has been validated in a study correlating MWF with a quantitative histopathologic measure of myelin density (Luxol fast blue myelin staining) in postmortem brain samples obtained from multiple sclerosis patients [41]. Overall, MWF showed a strong positive correlation with the Luxol fast blue staining, indicating that MWF is indeed a valid measure of myelin density in the human brain. Further validation also comes from a recent aging study [42].

The aim of the current study was to examine the effects of genetic variation in *PLP1*, a myelin-related gene, on white matter microstructure as assessed by myelin water fraction (MWF) imaging in the whole brain. As *PLP1* encodes for proteolipid protein 1, the predominant component of myelin, we hypothesized that genetic variation in *PLP1* should be linked to differences in MWF. As *PLP1* has previously been related to hemispheric asymmetries [13] and white matter microstructure is asymmetrically

organized on both the whole-brain level [1, 43] as well as in regard to specific tracts, e.g., the superior longitudinal fasciculus connecting the parietal and frontal lobes [44], we also specifically investigated this factor.

Methods

Participants

A cohort of 246 healthy adults (116 females and 130 males) were tested. Participants' ages ranged from 18 to 69 years, with a mean of 25.4 years. Most participants were university students, and all participants were of Caucasian descent for at least two generations, the majority of them being German. All participants had no history of psychiatric or neurological disorders and matched the standard inclusion criteria for MRI examinations. Information on their state of health was part of the demographic questionnaire and was therefore self-reported by the subjects. Of the 246 participants, 237 were right-handed and 19 were left-handed, as measured by the Edinburgh Handedness Inventory [45]. Self-reports ensured that participants were genetically unrelated to one another. The study was approved by the local ethics committee of the Faculty of Psychology at Ruhr University Bochum. All participants gave their written informed consent and were treated in accordance with the Declaration of Helsinki.

Genotyping

All participants contributed oral mucosa samples collected with buccal swabs. The QIAamp DNA kit (Qiagen, GmbH, Hilden, Germany) was used to isolate DNA from the exfoliated cells. Both polymerase chain reaction (PCR) and restriction fragment length polymorphisms (RFLP) were carried out to genotype the selected gene. Further details and primer sequences are available upon request. Previously, we found associations between myelin gene variation and interhemispheric integration [3]; from this, we focused on genotyping two different *PLP1* single nucleotide polymorphisms (SNPs): the synonymous exchange rs1126707 (c.609T>C [p.Asp203=]) and the intronic variation rs521895. ESEFinder [46] and RESCUE-ESE [47], both integrated in Alamut® Visual 2.8.1, were used to evaluate splicing regulatory elements.

Neuroimaging

All imaging data were acquired at the Bergmannsheil hospital in Bochum (Germany) using a Philips 3T Achieva whole-body MRI scanner with a 32-channel head coil.

Anatomical Imaging For the purpose of segmenting brain scans into gray and white matter as well as for the

identification of anatomical landmarks, a T1-weighted high-resolution anatomical image was acquired with a 3D-Inversion prepared Turbo Field echo—3D-IR-TFE (MPRAGE) using the following parameters: TR = 8.2 ms, TE = 3.7 ms, flip angle = 8°, inversion delay (min TI delay) = 617.7 ms, TFE shot duration = 1487 ms, 220 slices, matrix size = 240 × 240, and voxel size = 1 × 1 × 1 mm. The acquisition time of the anatomical image was 6 min.

Myelin Water Imaging We utilized a previously published 3D multi-echo gradient spin echo (3D ME-GRASE) sequence with refocusing angle sweep [29, 32] using the following parameters: TR = 800 ms; TE = 10, 20, 30, ..., 320 ms (32 echoes at 10 ms echo spacing); 60 slices; partial Fourier acquisition in both phase encoding directions; parallel imaging SENSE = 2.0; matrix size = 112 × 112; resolution = 2 × 2 × 2 mm; and a total acquisition time of 8 min.

Analysis of Data from Anatomical Imaging We used published surface-based methods in FreeSurfer (<http://surfer.nmr.mgh.harvard.edu>, version 5.3.0) to reconstruct the cortical surfaces of the T1-weighted images. The details of this procedure have been described elsewhere [48, 49]. The automatic reconstruction steps included skull stripping, gray and white matter segmentation, and reconstruction and inflation of the cortical surface. These processing steps were carried out for each individual participant. The resulting segmentations were controlled slice by slice, and any inaccuracies caused by the automatic processing were manually corrected if necessary. We selected a set of 33 brain regions per hemisphere to be examined with regard to asymmetries in myelination. We utilized an automatic segmentation procedure in FreeSurfer [50, 51] to delineate these regions within the white matter (Fig. 1). First, the reconstructed cortical surface was segmented into cortical gray matter regions following a gyral/sulcal-based parcellation procedure [52]. Second, corresponding white matter regions were defined by labeling each white matter voxel according to the nearest cortical gray matter voxel within a distance limit of 5 mm [50]. This resulted in 33 white matter regions corresponding to the 33 gyral-labeled gray matter regions. Third, in order to analyze the myelination of overall lobes, white matter regions were aggregated based on the cortical lobes constituted by their gray matter counterparts (occipital, temporal, parietal, frontal, and cingulate cortex). This aggregation followed a scheme described in [52]. Finally, the whole set of masks, delineating the overall white matter, its lobe regions, and the 33 brain regions defined by the Desikan-Killiany Atlas [52], was linearly transformed into the native space of myelin water images.

Analysis of Data from Myelin Water Imaging We created parameter maps representing the myelin water fraction (MWF) for each voxel (Fig. 1) from the 3D ME-GRASE sequence by

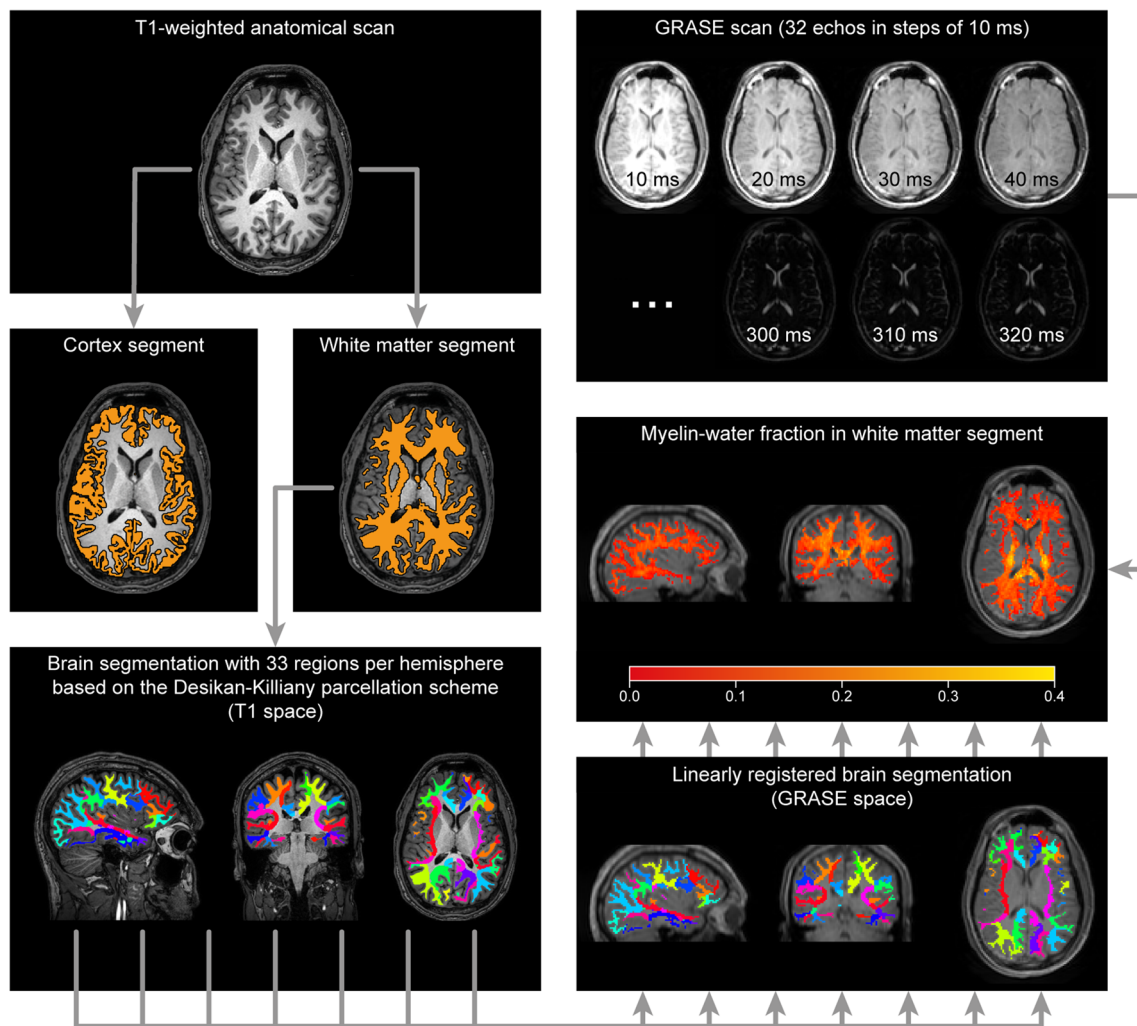


Fig. 1 Methodological sequence for the estimation of myelin water fraction within white matter regions. First, T1-weighted anatomical images were partitioned into two segments including the overall cortex and white matter of the brain, respectively. Second, the white matter segment was further partitioned into 33 regions per hemisphere based on the Desikan-Killiany Atlas implemented in FreeSurfer. White matter regions adjacent to the same cortical lobe were aggregated in order to create additional masks covering larger portions of white matter. Third,

parameter maps of myelin water fraction were computed by analyzing the multi-echo GRASE scans with an in-house MATLAB algorithm. Fourth, the whole set of masks, delineating the overall white matter, its lobe regions, and a total of 66 regions (33 in the left and 33 in the right hemisphere) as defined by the Desikan-Killiany Atlas, was linearly transformed into the native space of myelin water images. Fifth, mean values of myelin water fraction were computed for both overall white matter and each white matter region as defined by the set of masks

means of an in-house algorithm written in MATLAB (version 8.5.0.197613 (R2015a), The MathWorks Inc., Natick, MA). Multi-echo decay curves were analyzed on a voxel-wise base using multicomponent T2 analysis with concurrent correction for stimulated echo contamination of decay curves resulting from B1 inhomogeneity and imperfect refocusing pulses as outlined in [32].

The multi-echo (ME) decay curve was obtained for each voxel from the 3D ME-GRASE images and transformed into a continuous T2 distribution using a regularized non-negative least squares (NNLS) approach [42]. An extended phase graph algorithm was used to account for possible stimulated echoes due to non-ideal refocusing pulse flip angles [32, 53].

A 1.02 regularization factor was used during the fitting procedure to increase robustness of the ill-posed fitting problem and assure smooth T2 amplitude distributions. T2 distributions were created using 101 logarithmically spaced exponential decay base functions for the echo decay with T2 values ranging from 0.01 to 2 s. From the T2 distributions, the myelin water fraction (MWF) was calculated for each voxel as the signal integral fraction between 10 and 40 ms relative to the total T2 distribution integral (area under the curve). Example MWF parameter maps masked for white matter are depicted in Fig. 1. As a further step and as described above, the white matter masks defined from the T1-weighted anatomical scans were linearly transformed into the native space of the myelin water images to compute MWF coefficients for different masks across the whole white matter.

Statistical Analyses

The dependent variable used in the present study was the myelin water fraction (MWF) for the whole brain, five lobes, and 33 areas (as per the Desikan parcellation scheme) [50, 52]. Based on our previous analyses [3], a codominant effect for each polymorphism was assumed for all current statistical analyses. Thus, all genotype groups were analyzed separately. For both of the *PLP1* SNPs, separate 5 (genotype) \times 2 (hemisphere) repeated-measures ANOVAs were conducted. Genotype was used as the between-subjects variable (Greenhouse–Geisser corrected). As the *PLP1* gene is located on the X chromosome, there are two genotypes for males and three genotypes for females. Since we were interested in investigating the hemispheric differences in myelination for the whole brain, lobes, and the 33 areas, we used the individual hemispheres (left and right) as the within-subjects variable. Head size was integrated into the analyses as a covariate, as we found a difference in average head size between male ($M = 57.9$, $SD = 1.4$) and female ($M = 55.4$, $SD = 1.6$) participants, $t_{(244)} = 13.0$, $p < 0.001$, which could possibly indicate a difference in average brain size. Although linkage disequilibrium (LD) analyses showed moderately strong LDs between the two *PLP1* SNPs for both male ($r = -0.43$, $p < 0.001$) and female ($r = -0.42$, $p < 0.001$) participants, we continued our analyses using Bonferroni correction to correct for multiple comparisons. All significant effects are indicated as surviving Bonferroni correction for the number of SNPs multiplied by the number of brain regions ($2 \times 39 = 78$; $\alpha = 0.000641$).

Results

Genotype Distributions

For SNPs on the X chromosome, females carry two copies but males carry only one copy. Therefore, genotype percentages were calculated separately for male and female participants.

Altogether, 70.3% of males carried the common T genotype and 29.7% the C genotype. For females, 55.1% were genotyped homozygous TT, 37.3% heterozygous CT, and 7.6% homozygous CC. For male participants, the MAF for *PLP1* rs1126707 was 0.30, and 0.26 for female participants, resulting in a combined MAF of 0.28. The MAF reported for this SNP in dbSNP (<https://www.ncbi.nlm.nih.gov/projects/SNP/>) is 0.29, and therefore, the MAF observed in our cohort is in line with what would be expected in the population.

In the case of *PLP1* rs521895, 69.8% of males carried the common G genotype and 30.2% the A genotype. For females, 50.4% were genotyped homozygous GG, 42.7% heterozygous AG, and 6.8% homozygous AA. For male participants, the MAF for *PLP1* rs521895 was 0.30, and 0.28 for females, resulting in a combined MAF of 0.29, which is roughly in line with the reported MAF of 0.38 in the general population.

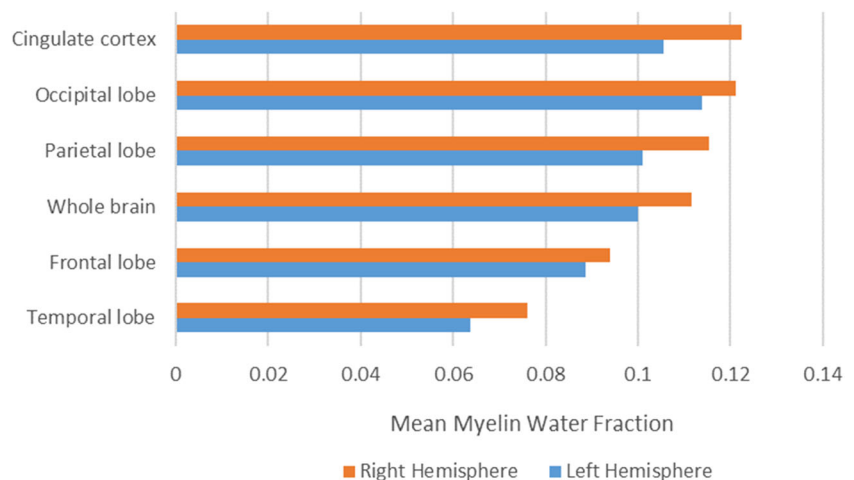
While submitting the sequence surrounding the two SNPs to the splicing regulatory analysis servers ESEFinder [44] and RESCUE-ESE [45], only ESEFinder predicted anything for rs1126707 (c.609T>C [p.Asp203=]). That prediction is that c.609C creates a new *SF2/ASF binding motif* (score 3.02), which raises the interesting possibility of impact on the regulatory level rather than the protein level.

Neuroimaging Results

Hemispheric Asymmetries in MWF

In order to examine general hemispheric differences in MWF across all areas, including the whole brain and lobes, Bonferroni-corrected paired-samples t tests were conducted. We found a significant rightward difference in MWF between the left and right hemispheres across the whole brain ($t_{(245)} = -36.36$, $p < 0.0001$) as well as for all four lobes (all $t_{(245)} > -6.08$, all p 's < 0.0001) and the cingulate cortex ($t_{(245)} = -$

Fig. 2 Average MWF for the right (orange) and the left (blue) hemisphere for the different lobes



23.71, $p < 0.0001$). That is, right hemisphere MWF was significantly greater than left hemisphere MWF for these areas (see Fig. 2).

For the 33 investigated areas, we also conducted Bonferroni-corrected paired-samples t tests to examine general hemispheric differences in MWF. Most areas demonstrated a significant difference in MWF between the left and right hemispheres (all $t_{(245)} > -3.73$, all p 's < 0.0001). The non-significant exceptions were the frontal pole ($t_{(245)} = 0.43$, $p = 0.67$) and the paracentral area ($t_{(245)} = 0.56$, $p = 0.58$). All significant hemispheric differences were rightward except for the cuneus, superior frontal, and medial orbitofrontal areas, which were leftward (see Fig. 3).

Association Between Genetic Variation and Neuroimaging Results

The results of all analyses investigating the effects of genetic variation on hemispheric asymmetries in MWF for the whole brain, lobes, and cingulate cortex are presented in Table 1, and Table 2 for the 33 areas. Further detailed analyses of all significant effects are described in the following subsections.

PLP1 rs1126707

For the whole brain, lobes, and cingulate cortex, we found no significant main effects of hemisphere (all F 's_(1,240) < 8.7 , all

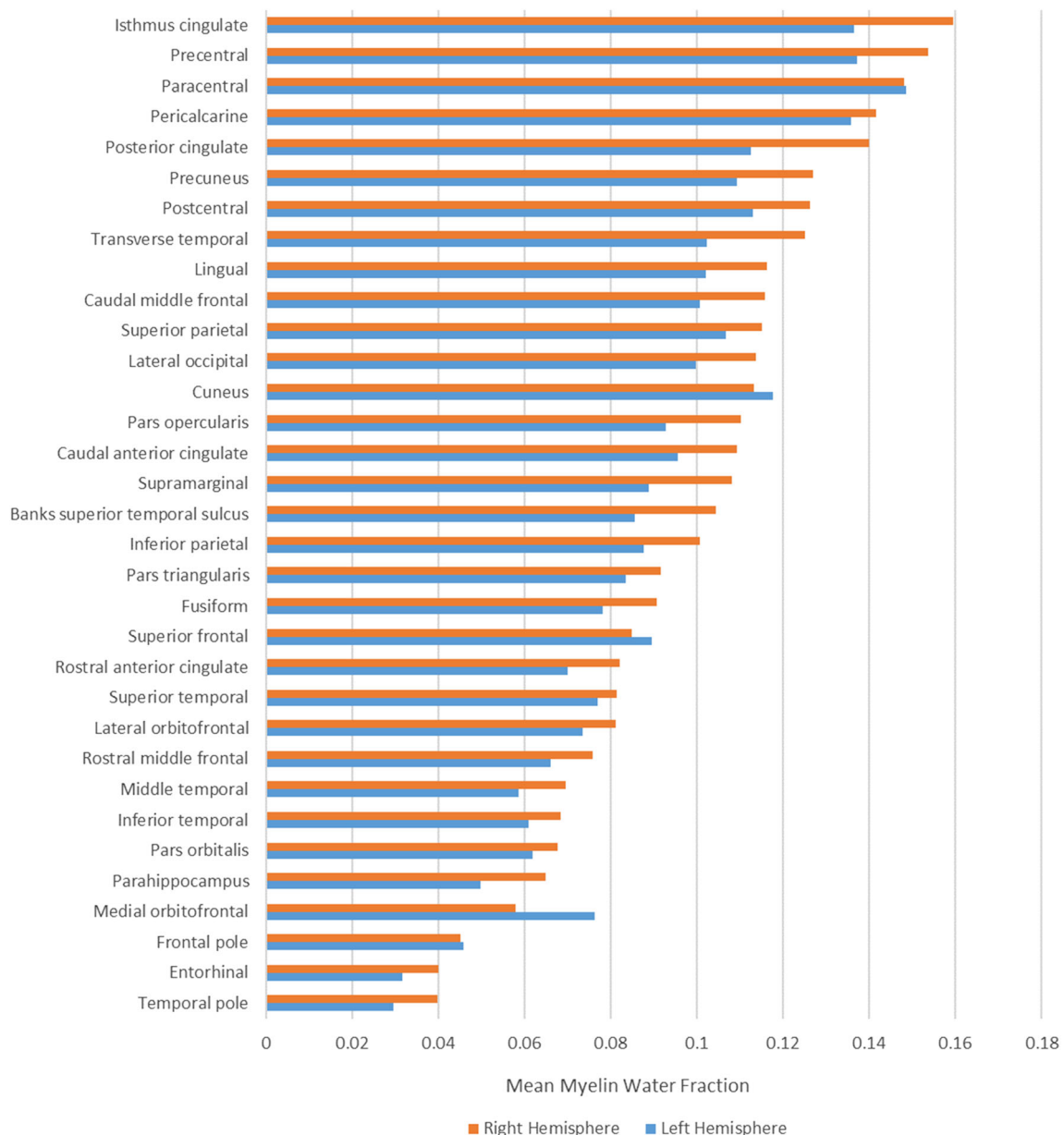


Fig. 3 Average MWF for the right (orange) and the left (blue) hemisphere for the different brain areas

Table 1 The association between genetic variation in *PLP1* and hemispheric asymmetries in MWF for the whole brain, the four lobes, and the cingulate cortex

Area	SNP	ME genotype	ME hemisphere	Interaction
Whole brain	<i>PLP1</i> rs1126707	<i>p</i> = 0.39	<i>p</i> = 0.97	<i>p</i> = 0.006
	<i>PLP1</i> rs521895	<i>p</i> = 0.58	<i>p</i> = 0.01	<i>p</i> = 0.01
Occipital lobe	<i>PLP1</i> rs1126707	<i>p</i> = 0.78	<i>p</i> = 0.93	<i>p</i> = 0.5
	<i>PLP1</i> rs521895	<i>p</i> = 0.43	<i>p</i> = 0.97	<i>p</i> = 0.24
Temporal lobe	<i>PLP1</i> rs1126707	<i>p</i> = 0.33	<i>p</i> = 0.40	<i>p</i> = 0.12
	<i>PLP1</i> rs521895	<i>p</i> = 0.81	<i>p</i> = 0.36	<i>p</i> = 0.24
Parietal lobe	<i>PLP1</i> rs1126707	<i>p</i> = 0.48	<i>p</i> = 0.31	<i>p</i> = 0.0000006
	<i>PLP1</i> rs521895	<i>p</i> = 0.59	<i>p</i> = 0.21	<i>p</i> = 0.000002
Frontal lobe	<i>PLP1</i> rs1126707	<i>p</i> = 0.2	<i>p</i> = 0.64	<i>p</i> = 0.06
	<i>PLP1</i> rs521895	<i>p</i> = 0.72	<i>p</i> = 0.69	<i>p</i> = 0.54
Cingulate cortex	<i>PLP1</i> rs1126707	<i>p</i> = 0.64	<i>p</i> = 0.003	<i>p</i> = 0.13
	<i>PLP1</i> rs521895	<i>p</i> = 0.81	<i>p</i> = 0.008	<i>p</i> = 0.015

Significant effects are shown in italics, after Bonferroni correction and the addition of head size as a covariate

p 's > 0.003) or genotype (all $F^2_{s(4,240)} < 1.47$, all p 's > 0.2). There was a significant interaction effect in the parietal lobe ($F_{(4,240)} = 9.19$, $p < 0.0001$) surviving Bonferroni correction (see Fig. 4a). For the remaining 33 areas, we found no significant main effects of genotype (all $F^2_{s(4,240)} < 2.24$, all p 's > 0.066). However, there was a significant main effect of hemisphere for the medial orbitofrontal ($F_{(1,240)} = 22.66$, $p < 0.0001$) and rostral anterior cingulate ($F_{(1,240)} = 29.41$, $p < 0.0001$) both surviving Bonferroni correction. There was also a significant interaction effect in the supramarginal gyrus ($F_{(4,240)} = 6.46$, $p < 0.0001$), surviving Bonferroni correction (see Fig. 4b).

To further investigate the interaction between hemisphere and genotype in the parietal lobe and supramarginal gyrus, we performed Bonferroni-corrected independent-samples t tests between the left and the right hemisphere for each genotype. For the parietal lobe, across all genotypes, there were significant differences in MWF between the left and right hemispheres (all p 's < 0.0001). This interaction effect is shown in Fig. 4a. In general, all genotypes showed a rightward MWF asymmetry, for both males and females. Within males, the strongest asymmetry in terms of absolute numbers was observed for the T genotype (right hemisphere MWF, 0.119; left hemisphere MWF, 0.102; difference, 0.0169), over the C genotype (right hemisphere, 0.114; left hemisphere, 0.0994; difference, 0.0145). In females, the strongest asymmetry was observed for the TT genotype (right, 0.114; left, 0.101; difference, 0.0129), followed by the CT genotype (right, 0.113; left, 0.999; difference, 0.0127) and the CC genotype (right, 0.115; left, 0.107; difference, 0.008).

For the supramarginal gyrus, across all genotypes, there were significant differences in MWF between the left and right hemispheres (all p 's < 0.0001). This interaction effect is shown in Fig. 4b. In general, all genotypes showed a rightward MWF asymmetry, for both males and females. Within males, the strongest asymmetry in terms of absolute numbers

was observed for the T genotype (right, 0.112; left, 0.0893; difference, 0.0224), over the C genotype (right, 0.106; left, 0.0889; difference, 0.0181). In females, the strongest asymmetry was observed for the CT genotype (right, 0.105; left, 0.0866; difference, 0.0182), followed by the TT genotype (right, 0.106; left, 0.0889; difference, 0.0174) and the CC genotype (right, 0.108; left, 0.0939; difference, 0.0142).

***PLP1* rs521895**

For the whole brain, lobes, and cingulate cortex, we found no significant main effects of hemisphere (all $F^2_{s(1,240)} < 7.15$, all p 's > 0.008) or genotype (all $F^2_{s(4,240)} < 0.96$, all p 's > 0.43). There was a significant interaction effect in the parietal lobe ($F_{(4,240)} = 6.48$, $p < 0.0001$) surviving Bonferroni correction. For the remaining 33 areas, we found no significant main effects of genotype (all $F^2_{s(4,240)} < 2.16$, all p 's > 0.074). However, there was a significant main effect of hemisphere for the medial orbitofrontal ($F_{(1,240)} = 22.63$, $p < 0.0001$) and rostral anterior cingulate ($F_{(1,240)} = 27.57$, $p < 0.0001$) both surviving Bonferroni correction. There was also a significant interaction effect in the postcentral area ($F_{(4,240)} = 5.37$, $p = 0.0004$) surviving Bonferroni correction.

To further explore the hemisphere by genotype interaction in the parietal lobe and postcentral area, we performed Bonferroni-corrected independent-samples t tests between the left and the right hemisphere for each genotype. For the parietal lobe, across all genotypes, there were significant differences in MWF between the left and right hemispheres (all p 's < 0.0001). This interaction effect is shown in Fig. 5a. In general, all genotypes showed a rightward MWF asymmetry, for both males and females. Within males, the strongest asymmetry in terms of absolute numbers was observed for the A genotype (right hemisphere MWF, 0.116; left hemisphere MWF, 0.0984; difference, 0.0174), over the G genotype (right hemisphere, 0.119; left hemisphere, 0.103; difference,

Table 2 The association between genetic variation in *PLP1* and hemispheric asymmetries in MWF for the 33 investigated brain areas

Area	SNP	ME genotype	ME hemisphere	Interaction
Banks superior temporal sulcus	<i>PLP1</i> rs1126707	$p = 0.21$	$p = 0.56$	$p = 0.18$
	<i>PLP1</i> rs521895	$p = 0.6$	$p = 0.62$	$p = 0.7$
Caudal anterior cingulate	<i>PLP1</i> rs1126707	$p = 0.58$	$p = 0.024$	$p = 0.05$
	<i>PLP1</i> rs521895	$p = 0.11$	$p = 0.04$	$p = 0.019$
Caudal middle frontal	<i>PLP1</i> rs1126707	$p = 0.5$	$p = 0.79$	$p = 0.1$
	<i>PLP1</i> rs521895	$p = 0.32$	$p = 0.79$	$p = 0.081$
Cuneus	<i>PLP1</i> rs1126707	$p = 0.61$	$p = 0.28$	$p = 0.19$
	<i>PLP1</i> rs521895	$p = 0.42$	$p = 0.3$	$p = 0.55$
Entorhinal	<i>PLP1</i> rs1126707	$p = 0.43$	$p = 0.97$	$p = 0.77$
	<i>PLP1</i> rs521895	$p = 0.31$	$p = 0.77$	$p = 0.36$
Frontal pole	<i>PLP1</i> rs1126707	$p = 0.26$	$p = 0.77$	$p = 0.5$
	<i>PLP1</i> rs521895	$p = 0.22$	$p = 0.79$	$p = 0.99$
Fusiform	<i>PLP1</i> rs1126707	$p = 0.68$	$p = 0.039$	$p = 0.43$
	<i>PLP1</i> rs521895	$p = 0.33$	$p = 0.053$	$p = 0.19$
Inferior parietal	<i>PLP1</i> rs1126707	$p = 0.39$	$p = 0.002$	$p = 0.001$
	<i>PLP1</i> rs521895	$p = 0.82$	$p = 0.003$	$p = 0.016$
Inferior temporal	<i>PLP1</i> rs1126707	$p = 0.54$	$p = 0.35$	$p = 0.28$
	<i>PLP1</i> rs521895	$p = 0.72$	$p = 0.38$	$p = 0.61$
Isthmus cingulate	<i>PLP1</i> rs1126707	$p = 0.57$	$p = 0.83$	$p = 0.085$
	<i>PLP1</i> rs521895	$p = 0.88$	$p = 0.56$	$p = 0.009$
Lateral occipital	<i>PLP1</i> rs1126707	$p = 0.62$	$p = 0.26$	$p = 0.4$
	<i>PLP1</i> rs521895	$p = 0.64$	$p = 0.39$	$p = 0.14$
Lateral orbitofrontal	<i>PLP1</i> rs1126707	$p = 0.032$	$p = 0.96$	$p = 0.46$
	<i>PLP1</i> rs521895	$p = 0.66$	$p = 0.79$	$p = 0.25$
Lingual	<i>PLP1</i> rs1126707	$p = 0.9$	$p = 0.96$	$p = 0.39$
	<i>PLP1</i> rs521895	$p = 0.56$	$p = 0.97$	$p = 0.13$
Medial orbitofrontal	<i>PLP1</i> rs1126707	$p = 0.11$	$p = 0.000003$	$p = 0.96$
	<i>PLP1</i> rs521895	$p = 0.84$	$p = 0.000003$	$p = 0.71$
Middle temporal	<i>PLP1</i> rs1126707	$p = 0.46$	$p = 0.34$	$p = 0.97$
	<i>PLP1</i> rs521895	$p = 0.7$	$p = 0.19$	$p = 0.42$
Parahippocampal	<i>PLP1</i> rs1126707	$p = 0.68$	$p = 0.5$	$p = 0.01$
	<i>PLP1</i> rs521895	$p = 0.61$	$p = 0.56$	$p = 0.073$
Paracentral	<i>PLP1</i> rs1126707	$p = 0.07$	$p = 0.001$	$p = 0.26$
	<i>PLP1</i> rs521895	$p = 0.074$	$p = 0.001$	$p = 0.63$
Pars opercularis	<i>PLP1</i> rs1126707	$p = 0.41$	$p = 0.007$	$p = 0.4$
	<i>PLP1</i> rs521895	$p = 0.69$	$p = 0.003$	$p = 0.21$
Pars orbitalis	<i>PLP1</i> rs1126707	$p = 0.033$	$p = 0.038$	$p = 0.058$
	<i>PLP1</i> rs521895	$p = 0.49$	$p = 0.028$	$p = 0.57$
Pars triangularis	<i>PLP1</i> rs1126707	$p = 0.11$	$p = 0.02$	$p = 0.42$
	<i>PLP1</i> rs521895	$p = 0.53$	$p = 0.016$	$p = 0.28$
Pericalcarine	<i>PLP1</i> rs1126707	$p = 0.85$	$p = 0.6$	$p = 0.61$
	<i>PLP1</i> rs521895	$p = 0.3$	$p = 0.61$	$p = 0.37$
Postcentral	<i>PLP1</i> rs1126707	$p = 0.59$	$p = 0.71$	$p = 0.003$
	<i>PLP1</i> rs521895	$p = 0.53$	$p = 0.69$	$p = 0.0004$
Posterior cingulate	<i>PLP1</i> rs1126707	$p = 0.52$	$p = 0.58$	$p = 0.12$
	<i>PLP1</i> rs521895	$p = 0.93$	$p = 0.66$	$p = 0.027$
Precentral	<i>PLP1</i> rs1126707	$p = 0.32$	$p = 0.17$	$p = 0.004$
	<i>PLP1</i> rs521895	$p = 0.35$	$p = 0.1$	$p = 0.007$
Precuneus	<i>PLP1</i> rs1126707	$p = 0.66$	$p = 0.17$	$p = 0.011$

Table 2 (continued)

Area	SNP	ME genotype	ME hemisphere	Interaction
Rostral anterior cingulate	<i>PLP1</i> rs521895	<i>p</i> = 0.31	<i>p</i> = 0.17	<i>p</i> = 0.17
	<i>PLP1</i> rs1126707	<i>p</i> = 0.066	<i>p</i> = 0.0000001	<i>p</i> = 0.29
Rostral middle frontal	<i>PLP1</i> rs521895	<i>p</i> = 0.95	<i>p</i> < 0.0001	<i>p</i> = 0.33
	<i>PLP1</i> rs1126707	<i>p</i> = 0.41	<i>p</i> = 0.19	<i>p</i> = 0.017
Superior frontal	<i>PLP1</i> rs521895	<i>p</i> = 0.46	<i>p</i> = 0.36	<i>p</i> = 0.4
	<i>PLP1</i> rs1126707	<i>p</i> = 0.56	<i>p</i> = 0.43	<i>p</i> = 0.006
Superior parietal	<i>PLP1</i> rs521895	<i>p</i> = 0.22	<i>p</i> = 0.29	<i>p</i> = 0.13
	<i>PLP1</i> rs1126707	<i>p</i> = 0.43	<i>p</i> = 0.64	<i>p</i> = 0.01
Superior temporal	<i>PLP1</i> rs521895	<i>p</i> = 0.6	<i>p</i> = 0.31	<i>p</i> = 0.001
	<i>PLP1</i> rs1126707	<i>p</i> = 0.3	<i>p</i> = 0.25	<i>p</i> = 0.26
Supramarginal	<i>PLP1</i> rs521895	<i>p</i> = 0.56	<i>p</i> = 0.32	<i>p</i> = 0.22
	<i>PLP1</i> rs1126707	<i>p</i> = 0.44	<i>p</i> = 0.19	<i>p</i> = 0.000059
Temporal pole	<i>PLP1</i> rs521895	<i>p</i> = 0.76	<i>p</i> = 0.08	<i>p</i> = 0.001
	<i>PLP1</i> rs1126707	<i>p</i> = 0.66	<i>p</i> = 0.48	<i>p</i> = 0.045
Transverse temporal	<i>PLP1</i> rs521895	<i>p</i> = 0.22	<i>p</i> = 0.46	<i>p</i> = 0.43
	<i>PLP1</i> rs1126707	<i>p</i> = 0.38	<i>p</i> = 0.83	<i>p</i> = 0.31
	<i>PLP1</i> rs521895	<i>p</i> = 0.78	<i>p</i> = 0.68	<i>p</i> = 0.12

Significant effects are shown in italics, after Bonferroni correction and the addition of head size as a covariate

0.0156). In females, the strongest asymmetry was observed for the GG genotype (right, 0.112; left, 0.0996; difference, 0.0129), followed by the AA genotype (right, 0.112; left, 0.1; difference, 0.0122) and the AG genotype (right, 0.114; left, 0.102; difference, 0.012).

For the postcentral area, across all genotypes, there were significant differences in MWF between the left and right hemispheres (all *p*'s < 0.008). This interaction effect is shown in Fig. 5b. In general, all genotypes showed a rightward MWF

asymmetry, for both males and females. Within males, the strongest asymmetry in terms of absolute numbers was observed for the A genotype (right, 0.126; left, 0.11; difference, 0.0164), over the G genotype (right, 0.13; left, 0.115; difference, 0.0149). In females, the strongest asymmetry was observed for the GG genotype (right, 0.123; left, 0.111; difference, 0.0125), followed by the AG genotype (right, 0.124; left, 0.114; difference, 0.0101) and the AA genotype (right, 0.121; left, 0.114; difference, 0.00659).

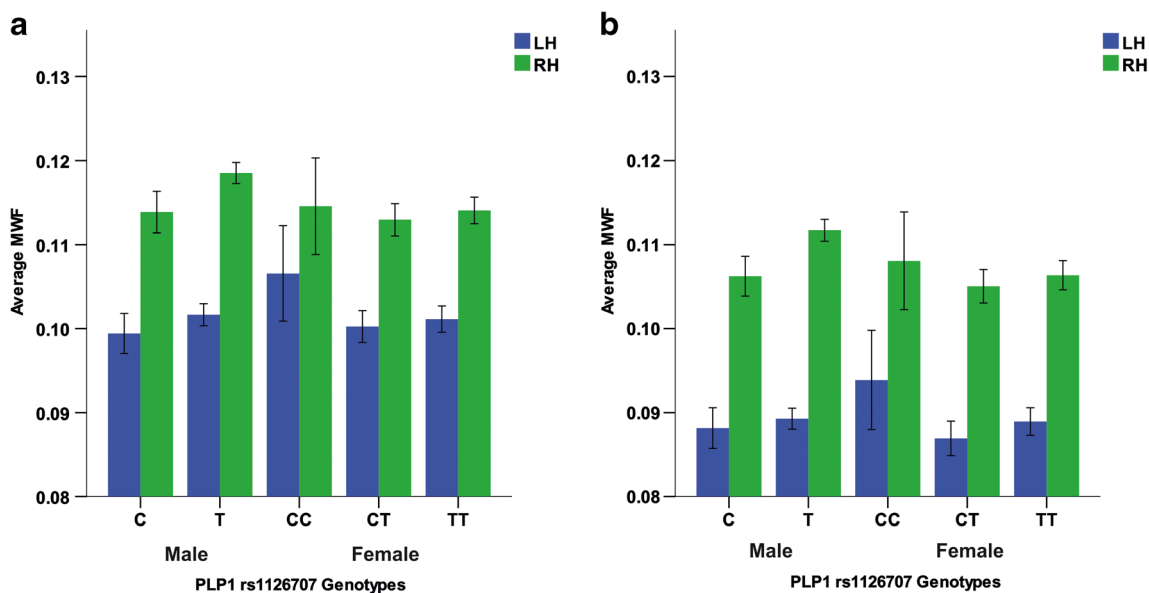


Fig. 4 Average MWF in relation to *PLP1* rs1126707 genotype for the parietal lobe (a) and the supramarginal gyrus (b). Error bars show standard error

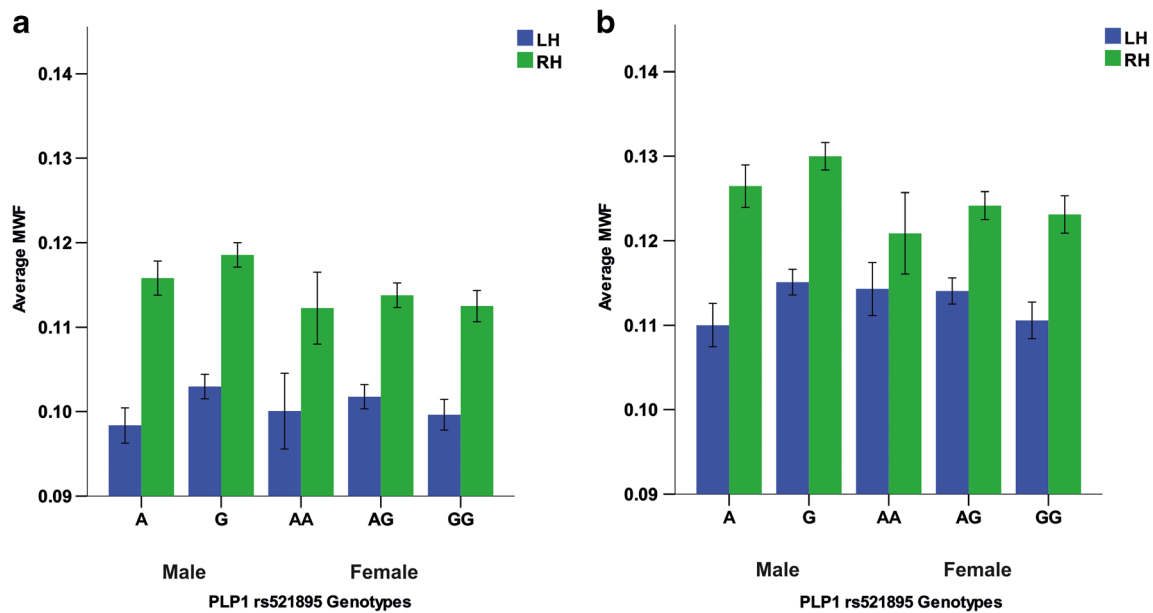


Fig. 5 Average MWF in relation to *PLP1* rs521895 genotype for the parietal lobe (a) and the postcentral gyrus (b). Error bars show standard error

Age Effects

As age has been shown to affect brain structure and brain myelin content, we re-analyzed the four significant analyses with age as a covariate. For the *PLP1* rs1126707 SNP, the genotype by hemisphere interaction remained significant for the parietal lobe ($F_{(4,239)} = 9.545$; $p < 0.0001$) as well as for the supramarginal gyrus ($F_{(4,239)} = 6.738$; $p < 0.0001$). For both analyses, the main effect of age also reached significance (parietal lobe: $F_{(1,239)} = 28.612$, $p < 0.0001$; supramarginal gyrus: $F_{(1,239)} = 27.105$, $p < 0.0001$). For the *PLP1* rs521895 SNP, the genotype by hemisphere interaction remained significant for the parietal lobe ($F_{(4,239)} = 6.736$; $p < 0.0001$) as well as for the postcentral gyrus ($F_{(4,239)} = 5.397$; $p < 0.001$). For both analyses, the main effect of age also reached significance (parietal lobe: $F_{(1,239)} = 28.342$; $p < 0.0001$; postcentral gyrus: $F_{(1,239)} = 26.431$, $p < 0.0001$).

These effects show that age has an effect on MWF, but does not specifically affect the relation between *PLP1* and hemispheric asymmetries. However, it also needs to be noted that the large majority of our sample was younger than 40, and only 14 participants were older than 40. Thus, for proper aging research on MWF, a sample with a much bigger group of older adults needs to be tested before any final conclusions can be drawn.

Discussion

The aim of the present study was to investigate hemispheric asymmetries in white matter as assessed by myelin water

fraction (MWF) imaging and study its association with genetic variation in the myelin-associated gene *PLP1*.

First, we systematically assessed hemispheric asymmetries in MWF across the whole brain. We found that for the whole brain, there was a rightward asymmetry in MWF, suggesting a higher content of myelin in the right hemisphere than in the left. This finding is in line with a xenon-133 inhalation study that investigated differences in the distribution of gray and white matter between the left and right hemisphere [43]. In 36 right-handed male undergraduate students, Gur et al. [43] found a higher ratio of gray to white matter in the left hemisphere than in the right, and a higher ratio of white to gray matter in the right hemisphere than in the left. Gur et al. [43] concluded that in absolute terms, there is likely more white matter in the right hemisphere and more gray matter in the left hemisphere. These findings were later confirmed by a large-scale neuroimaging study by Chiarello et al. [54], who found that in a sample of 100 men and 100 women, participants had on average 2% more white matter in the right hemisphere than in the left. The strongest MWF asymmetries were found in the cingulate cortex and parietal lobe, followed by the temporal lobe, frontal lobe, and occipital lobe.

We also investigated MWF asymmetries in 33 separate brain areas following the Desikan parcellation scheme [50, 52]. Here, we found both leftward and rightward MWF asymmetries, with rightward asymmetries being more prominent than leftward asymmetries. Significant leftward asymmetries were located in the cuneus, superior frontal, and medial orbitofrontal areas. Leftward MWF asymmetry in the medial orbitofrontal cortex might correspond to leftward asymmetry of the uncinate fasciculus as reported by DTI studies [22, 55]. The uncinate fasciculus is a white matter

tract that connects the anterior temporal lobe with the orbitofrontal cortex and has been implicated in language and emotion [56]. For the cuneus and superior frontal cortex, there do not seem to be direct equivalents in DTI studies investigating hemispheric asymmetries. In general, our findings do not show a substantial overlap with FA-based studies on hemispheric asymmetries in white matter [57, 58]. In general, those show a larger amount of leftward FA asymmetries than the leftward MWF asymmetries that we found in our study. This highlights the importance of using MWF imaging for neurogenetic studies on myelin gene function, as these differences might have been caused by the fact that FA in white matter reflects not only myelin, but is influenced by a number of other factors, including axon diameter and packing density, axon permeability, and fiber geometry [28–31].

Due to its strong correspondence with histological studies, the MWF technique therefore seems to be the most suitable non-invasive in vivo method to use in human studies, particularly when characterizing the quantity and integrity of axonal sheaths in a myelin-specific manner [38]. Although other MR methods do exist to address the integrity of white matter (such as magnetization transfer [59], diffusion anisotropy [25], or neurite orientation dispersion; NODDI) [60, 61], these methods tend to be more strongly influenced by other factors than myelin content [38, 62, 63].

To the best of our knowledge, there are no previously published papers investigating MWF asymmetries at the brain area level in healthy adults, and therefore, this study is the first to do so. However, O'Muircheartaigh et al. [64] recently published a study investigating MWF asymmetries in a sample of 108 typically developing children aged between 1 and 6 years. Unlike our study, these authors did not use predetermined brain regions for the asymmetry analysis, but conducted a voxel-wise comparison and then determined clusters with significant asymmetries. Subsequently, the brain areas covered by these clusters were ascertained. Similar to our results, O'Muircheartaigh et al. [64] found both leftward and rightward MWF asymmetries, but with a somewhat more leftward bias than in our study. Overall, clusters showing significant rightward asymmetry were located in the extreme capsule, the white matter underlying lateral motor cortex, and the ventral frontal cortex. Clusters showing significant leftward MWF asymmetry were located in the anterior caudate and thalamus, medial frontal cortex, posterior parietal lobe, and the arcuate fasciculus. These differences between the study by O'Muircheartaigh and our work can be partly explained by methodological differences, but are probably mostly due to developmental changes in white matter, as this continues to develop up until middle adulthood [65, 66].

In a second step, we investigated the association between the two *PLP1* SNPs, rs1126707 and rs521895, and hemispheric asymmetries in MWF for the whole brain, lobes, cingulate cortex, and 33 separate brain areas. Overall, the

genotype distributions for our sample were in line with the expected population frequencies based on the dbSNP database. We found that both SNPs showed significant associations with hemispheric asymmetries in MWF.

For *PLP1* rs1126707, we found a significant hemisphere-by-genotype interaction for both the parietal lobe on the lobe level and the supramarginal gyrus on the area level. The supramarginal gyrus is located in the parietal lobe. Thus, it can be assumed that the association between the alleles of this polymorphism and MWF asymmetries in the parietal lobe is driven by this area. Bonferroni-corrected post hoc tests showed that all rs1126707 genotypes showed significant rightward MWF asymmetries in the parietal lobe. In absolute MWF values, males with the common T allele showed stronger MWF asymmetries in the parietal lobe than males with the rare C allele. For females, the homozygous TT genotype carrier showed the strongest asymmetries, followed by the heterozygous CT genotypes and rare homozygous CC genotypes. Women with the CC genotype had the overall weakest asymmetries in absolute terms, even when compared with the males with the C genotype. Thus, the rare rs1126707 C allele seems to lead to decreased MWF asymmetries in the parietal lobe.

In line with this result, Bonferroni-corrected post hoc tests showed that all rs1126707 genotypes showed significant rightward MWF asymmetries in the supramarginal gyrus. As with the parietal lobe, males with the T allele had stronger asymmetries than males with the C allele. For female participants, the strongest asymmetries were observed for the CT genotypes, followed by the homozygous TT and CC genotypes. With respect to heterozygous females, it should be noted that most loci on the X chromosome are subject to X inactivation in females, meaning that only one allele from each pair of alleles is expressed [67]. However, the inactivated allele in each cell is selected at random. Therefore, it is unknown which of the two alleles is expressed in heterozygous females. Nevertheless, women with the CC genotype showed the overall weakest asymmetries of all participants. Thus, in line with our overall parietal lobe findings, the rare rs1126707 C allele seems to lead to decreased MWF asymmetries in the supramarginal gyrus.

Therefore, we conclude that the rare C allele is associated with a reduction in hemispheric asymmetries. This association between the rare C allele and reduced hemispheric asymmetry has also been observed in a study involving the dichotic listening task, which is used to assess language lateralization [68–71]. Moreover, individuals with the rare rs1126707 C allele have been shown to have altered interhemispheric processing compared to other individuals [3]. While we can only speculate why we found a specific effect for the supramarginal gyrus, it is striking that the white matter underlying this area is a part of the superior longitudinal fasciculus (SLF). The SLF is a large white matter tract connecting the frontal and parietal lobes that has been implicated in visuo-spatial attention and shows a strong rightward structural asymmetry [44]. This

asymmetry is one of the strongest rightward structural white matter asymmetries that have been observed in DTI studies [44]. Therefore, it makes sense that genetic variation in a myelin-related gene like *PLP1* affects the structure of this area.

For *PLP1* rs521895, we also found a significant hemisphere-by-genotype interaction for both the parietal lobe on the lobe level and the postcentral gyrus on the area level. The postcentral gyrus is located in the parietal lobe. Thus, it can be assumed that the association between genetic variations in *PLP1* rs521895 and MWF asymmetries in the parietal lobe is driven by this area. Here, Bonferroni-corrected post hoc tests showed that all rs521895 genotypes showed significant rightward MWF asymmetries in the parietal lobe. However, in terms of absolute MWF asymmetries, the association varies between male and female participants. Here, males carrying the rare A allele showed stronger MWF asymmetries than males with the G allele. For females, the strongest asymmetry is associated with the common homozygous GG genotype, followed by the homozygous AA genotype and the heterozygous AG genotype. Bonferroni-corrected post hoc tests also showed that all rs521895 genotypes showed significant rightward MWF asymmetries in the postcentral gyrus. In line with the results for the parietal lobe, males with the rare A allele showed stronger asymmetries than males with the G allele. For females, the strongest asymmetry was observed in the GG genotype, followed by the AG genotype and the AA genotype. Thus, for rs521895, the rare A allele leads to reduced MWF asymmetries in the parietal lobe and the postcentral gyrus for females, but not for males. Furthermore, for the rs521895 SNP, we found a specific effect for the postcentral area. As with the supramarginal gyrus which was associated with genetic variation in the rs1126707 SNP, this brain area is located in the parietal lobe. It has been related to somatosensory processing, and like the supramarginal gyrus, the white matter underlying it is part of the SLF.

The function of *PLP1* has not been fully established. However, its implication in myelination and the fact that the amino acid sequence of *PLP* has been highly conserved during mammalian evolution [72] increases the probability that *PLP1* sequence variation may impact white matter size or structure, which in turn is likely to significantly affect brain function. Unfortunately, it is not known whether the polymorphisms analyzed are functional. However, the results generated by ESE finder [46] indicated that the c.609C nucleotide of the synonymous SNP rs1126707 that induces no amino acid change creates a new SF2/ASF binding motif (score 3.02). However, the RESCUE-ESE program [47] did not show any difference between the distribution of exonic splicing enhancers (ESE) motifs in the wild-type and the variant sequence. ESEs stimulate splicing and serve as binding sites for various splicing factors, of which the best characterized are the serine/arginine-rich proteins (SR proteins) [73]. Therefore, the C allele of SNP rs1126707 may lead to changes

in the splicing pattern with functional consequences that could potentially affect brain structure. Future studies should focus on the exact nature of these potential functional consequences of genetic variation in this allele. Moreover, future studies should use other myelin-specific MRI measures than MWF, such as magnetization transfer imaging, mcDESPOT, and radial diffusivity [38], to investigate the neurogenetics of *PLP1*.

Taken together, the results of the present study suggest the existence of mostly rightward MWF asymmetries in the adult human brain. Importantly, genetic variation in the myelin-associated gene *PLP1* affects MWF asymmetries in the parietal lobe. Potentially, these rightward structural asymmetries are related to previously reported rightward structural asymmetries in the SLF.

Acknowledgements The authors thank Martijn Froeling and PHILIPS Germany for their scientific support with the MRI measurements as well as Tobias Otto for his technical support.

Funding Information This work was supported by the Deutsche Forschungsgemeinschaft (DFG) grant numbers Gu227/16-1 and GE2777/2-1 and the MERCUR foundation grant number An-2015-0044.

Compliance with Ethical Standards

The study was approved by the local ethics committee of the Faculty of Psychology at Ruhr University Bochum. All participants gave their written informed consent and were treated in accordance with the Declaration of Helsinki.

References

- Ocklenburg S, Güntürkün O (2018) The lateralized brain: the neuroscience and evolution of hemispheric asymmetries. Academic Press, London
- Filley C (2012) The behavioral neurology of white matter, 2nd edn. Oxford University Press USA, Oxford
- Ocklenburg S, Gerding WM, Arning L, Genç E, Epplen JT, Güntürkün O, Beste C (2017) Myelin genes and the corpus callosum: proteolipid protein 1 (PLP1) and contactin 1 (CNTN1) gene variation modulates interhemispheric integration. *Mol Neurobiol* 54(10):7908–7916. <https://doi.org/10.1007/s12035-016-0285-5>
- Friedrich P, Ocklenburg S, Heins N, Schlüter C, Fraenz C, Beste C, Güntürkün O, Genç E (2017) Callosal microstructure affects the timing of electrophysiological left-right differences. *Neuroimage* 163:310–318. <https://doi.org/10.1016/j.neuroimage.2017.09.048>
- Krämer EM, Schardt A, Nave KA (2001) Membrane traffic in myelinating oligodendrocytes. *Microsc Res Tech* 52(6):656–671. <https://doi.org/10.1002/jemt.1050>
- Boiko T, Winckler B (2006) Myelin under construction—teamwork required. *J Cell Biol* 172(6):799–801. <https://doi.org/10.1083/jcb.200602101>
- Laule C, Vavasour IM, Kolind SH, Li DKB, Traboulsee TL, Moore GRW, MacKay AL (2007) Magnetic resonance imaging of myelin. *Neurotherapeutics* 4(3):460–484. <https://doi.org/10.1016/j.nurt.2007.05.004>
- Griffiths I, Klugmann M, Anderson T, Thomson C, Vouyiouklis D, Nave KA (1998) Current concepts of PLP and its role in the

- nervous system. *Microsc Res Tech* 41(5):344–358. [https://doi.org/10.1002/\(SICI\)1097-0029\(19980601\)41:5<344::AID-JEMT2>3.0.CO;2-Q](https://doi.org/10.1002/(SICI)1097-0029(19980601)41:5<344::AID-JEMT2>3.0.CO;2-Q)
9. Yool DA, Klugmann M, McLaughlin M, Vouyiouklis DA, Dimou L, Barrie JA, McCulloch MC, Nave KA et al (2001) Myelin proteolipid proteins promote the interaction of oligodendrocytes and axons. *J Neurosci Res* 63(2):151–164. [https://doi.org/10.1002/1097-4547\(20010115\)63:2<151::AID-JNR1007>3.0.CO;2-Y](https://doi.org/10.1002/1097-4547(20010115)63:2<151::AID-JNR1007>3.0.CO;2-Y)
 10. Chow E, Mottahedeh J, Prins M, Ridder W, Nusinowitz S, Bronstein JM (2005) Disrupted compaction of CNS myelin in an OSP/Claudin-11 and PLP/DM20 double knockout mouse. *Mol Cell Neurosci* 29(3):405–413. <https://doi.org/10.1016/j.mcn.2005.03.007>
 11. Patzig J, Kusch K, Fledrich R, Eichel MA, Lüders KA, Möbius W, Sereda MW, Nave KA et al (2016) Proteolipid protein modulates preservation of peripheral axons and premature death when myelin protein zero is lacking. *Glia* 64(1):155–174. <https://doi.org/10.1002/glia.22922>
 12. Harlow DE, Saul KE, Culp CM, Vesely EM, Macklin WB (2014) Expression of proteolipid protein gene in spinal cord stem cells and early oligodendrocyte progenitor cells is dispensable for normal cell migration and myelination. *J Neurosci* 34(4):1333–1343. <https://doi.org/10.1523/JNEUROSCI.2477-13.2014>
 13. Ocklenburg S, Gerding WM, Raane M, Aming L, Genç E, Epplen JT, Güntürkün O, Beste C (2018) PLP1 gene variation modulates leftward and rightward functional hemispheric asymmetries. *Mol Neurobiol* 55:7691–7700. <https://doi.org/10.1007/s12035-018-0941-z>
 14. Fagerberg L, Hallström BM, Oksvold P, Kampf C, Djureinovic D, Odeberg J, Habuka M, Tahmasebpoor S et al (2014) Analysis of the human tissue-specific expression by genome-wide integration of transcriptomics and antibody-based proteomics. *Mol Cell Proteomics* 13(2):397–406. <https://doi.org/10.1074/mcp.M113.035600>
 15. Wight PA (2017) Effects of intron 1 sequences on human PLP1 expression: implications for PLP1-related disorders. *ASN Neuro* 9(4):1759091417720583. <https://doi.org/10.1177/1759091417720583>
 16. Ruest T, Holmes WM, Barrie JA, Griffiths IR, Anderson TJ, Dewar D, Edgar JM (2011) High-resolution diffusion tensor imaging of fixed brain in a mouse model of Pelizaeus-Merzbacher disease: comparison with quantitative measures of white matter pathology. *NMR Biomed* 24(10):1369–1379. <https://doi.org/10.1002/nbm.1700>
 17. Smith SM, Jenkinson M, Johansen-Berg H, Rueckert D, Nichols TE, Mackay CE, Watkins KE, Ciccarelli O et al (2006) Tract-based spatial statistics: voxelwise analysis of multi-subject diffusion data. *Neuroimage* 31(4):1487–1505. <https://doi.org/10.1016/j.neuroimage.2006.02.024>
 18. Dreha-Kulaczewski SF, Brockmann K, Henneke M, Dechent P, Wilken B, Gärtner J, Helms G (2012) Assessment of myelination in hypomyelinating disorders by quantitative MRI. *J Magn Reson Imaging* 36(6):1329–1338. <https://doi.org/10.1002/jmri.23774>
 19. Sumida K, Inoue K, Takanashi J-I, Sasaki M, Watanabe K, Suzuki M, Kurahashi H, Omata T et al (2016) The magnetic resonance imaging spectrum of Pelizaeus-Merzbacher disease: a multicenter study of 19 patients. *Brain and Development* 38(6):571–580. <https://doi.org/10.1016/j.braindev.2015.12.007>
 20. Takanashi J, Sugita K, Tanabe Y, Nagasawa K, Inoue K, Osaka H, Kohno Y (1999) MR-revealed myelination in the cerebral corticospinal tract as a marker for Pelizaeus-Merzbacher's disease with proteolipid protein gene duplication. *AJNR Am J Neuroradiol* 20(10):1822–1828
 21. Banich MT, Belger A (1990) Interhemispheric interaction: how do the hemispheres divide and conquer a task? *Cortex* 26(1):77–94
 22. Ocklenburg S, Friedrich P, Güntürkün O, Genç E (2016) Intrahemispheric white matter asymmetries: the missing link between brain structure and functional lateralization? *Rev Neurosci* 27(5):465–480. <https://doi.org/10.1515/revneuro-2015-0052>
 23. Tournier J-D, Mori S (eds) (2014) Introduction to diffusion tensor imaging: and higher order models, 2nd edn. Calif, Academic Press, Oxford, England, San Diego
 24. Behrens TEJ, Berg HJ, Jbabdi S, Rushworth MFS, Woolrich MW (2007) Probabilistic diffusion tractography with multiple fibre orientations: what can we gain? *Neuroimage* 34(1):144–155. <https://doi.org/10.1016/j.neuroimage.2006.09.018>
 25. Le Bihan D (2003) Looking into the functional architecture of the brain with diffusion MRI. *Nat Rev Neurosci* 4(6):469–480. <https://doi.org/10.1038/nrn1119>
 26. Pierpaoli C, Basser PJ (1996) Toward a quantitative assessment of diffusion anisotropy. *Magn Reson Med* 36(6):893–906
 27. Genç E, Ocklenburg S, Singer W, Güntürkün O (2015) Abnormal interhemispheric motor interactions in patients with callosal agenesis. *Behav Brain Res* 293:1–9. <https://doi.org/10.1016/j.bbr.2015.07.016>
 28. Zatorre RJ, Fields RD, Johansen-Berg H (2012) Plasticity in gray and white: neuroimaging changes in brain structure during learning. *Nat Neurosci* 15(4):528–536. <https://doi.org/10.1038/nn.3045>
 29. Mädler B, Drabycz SA, Kolind SH, Whittall KP, MacKay AL (2008) Is diffusion anisotropy an accurate monitor of myelination? Correlation of multicomponent T2 relaxation and diffusion tensor anisotropy in human brain. *Magn Reson Imaging* 26(7):874–888. <https://doi.org/10.1016/j.mri.2008.01.047>
 30. Beaulieu C (2002) The basis of anisotropic water diffusion in the nervous system—a technical review. *NMR Biomed* 15(7–8):435–455. <https://doi.org/10.1002/nbm.782>
 31. Mori S, Zhang J (2006) Principles of diffusion tensor imaging and its applications to basic neuroscience research. *Neuron* 51(5):527–539. <https://doi.org/10.1016/j.neuron.2006.08.012>
 32. Prasloski T, Rauscher A, MacKay AL et al (2012) Rapid whole cerebrum myelin water imaging using a 3D GRASE sequence. *Neuroimage* 63(1):533–539. <https://doi.org/10.1016/j.neuroimage.2012.06.064>
 33. Uddin MN, Figley TD, Marrie RA, Figley CR, for the CCOMS Study Group (2018) Can T1 w/T2 w ratio be used as a myelin-specific measure in subcortical structures? Comparisons between FSE-based T1 w/T2 w ratios, GRASE-based T1 w/T2 w ratios and multi-echo GRASE-based myelin water fractions. *NMR Biomed* 31(3). <https://doi.org/10.1002/nbm.3868>
 34. Whittall KP, MacKay AL, Graeb DA et al (1997) In vivo measurement of T2 distributions and water contents in normal human brain. *Magn Reson Med* 37(1):34–43
 35. Whittall KP, MacKay AL (1989) Quantitative interpretation of NMR relaxation data. *J Magn Reson* (1969) 84(1):134–152. [https://doi.org/10.1016/0022-2364\(89\)90011-5](https://doi.org/10.1016/0022-2364(89)90011-5)
 36. Laule C, Kozlowski P, Leung E, Li DKB, MacKay AL, Moore GRW (2008) Myelin water imaging of multiple sclerosis at 7 T: correlations with histopathology. *Neuroimage* 40(4):1575–1580. <https://doi.org/10.1016/j.neuroimage.2007.12.008>
 37. Meyers SM, Vavasour IM, Mädler B, Harris T, Fu E, Li DKB, Traboulsee AL, MacKay AL et al (2013) Multicenter measurements of myelin water fraction and geometric mean T2: intra- and intersite reproducibility. *J Magn Reson Imaging* 38(6):1445–1453. <https://doi.org/10.1002/jmri.24106>
 38. MacKay AL, Laule C (2016) Magnetic resonance of myelin water: an in vivo marker for myelin. *Brain Plast* 2(1):71–91. <https://doi.org/10.3233/BPL-160033>
 39. Alonso-Ortiz E, Levesque IR, Pike GB (2015) MRI-based myelin water imaging: a technical review. *Magn Reson Med* 73(1):70–81. <https://doi.org/10.1002/mrm.25198>
 40. Kroeker RM, Mark Henkelman R (1986) Analysis of biological NMR relaxation data with continuous distributions of relaxation

- times. *J Magn Reson* (1969) 69(2):218–235. [https://doi.org/10.1016/0022-2364\(86\)90074-0](https://doi.org/10.1016/0022-2364(86)90074-0)
41. Laule C, Leung E, Lis DKB et al (2006) Myelin water imaging in multiple sclerosis: quantitative correlations with histopathology. *Mult Scler* 12(6):747–753. <https://doi.org/10.1177/1352458506070928>
 42. Billiet T, Vandenbulcke M, Mädler B, Peeters R, Dhollander T, Zhang H, Deprez S, van den Bergh BRH et al (2015) Age-related microstructural differences quantified using myelin water imaging and advanced diffusion MRI. *Neurobiol Aging* 36(6):2107–2121. <https://doi.org/10.1016/j.neurobiolaging.2015.02.029>
 43. Gur RC, Packer IK, Hungerbühler JP, Reivich M, Obrist W, Amarek W, Sackeim H (1980) Differences in the distribution of gray and white matter in human cerebral hemispheres. *Science* 207(4436):1226–1228
 44. Thiebaut de Schotten M, Dell'Acqua F, Forkel SJ et al (2011) A lateralized brain network for visuospatial attention. *Nat Neurosci* 14(10):1245–1246. <https://doi.org/10.1038/nn.2905>
 45. Oldfield RC (1971) The assessment and analysis of handedness: the Edinburgh inventory. *Neuropsychologia* 9(1):97–113
 46. Cartegni L, Wang J, Zhu Z, Zhang MQ, Krainer AR (2003) ESEfinder: a web resource to identify exonic splicing enhancers. *Nucleic Acids Res* 31(13):3568–3571
 47. Fairbrother WG, Yeh R-F, Sharp PA, Burge CB (2002) Predictive identification of exonic splicing enhancers in human genes. *Science* 297(5583):1007–1013. <https://doi.org/10.1126/science.1073774>
 48. Dale AM, Fischl B, Sereno MI (1999) Cortical surface-based analysis. I. Segmentation and surface reconstruction. *Neuroimage* 9(2):179–194. <https://doi.org/10.1006/nimg.1998.0395>
 49. Fischl B, Sereno MI, Dale AM (1999) Cortical surface-based analysis. II: Inflation, flattening, and a surface-based coordinate system. *Neuroimage* 9(2):195–207. <https://doi.org/10.1006/nimg.1998.0396>
 50. Salat DH, Greve DN, Pacheco JL et al (2009) Regional white matter volume differences in nondemented aging and Alzheimer's disease. *Neuroimage* 44(4):1247–1258. <https://doi.org/10.1016/j.neuroimage.2008.10.030>
 51. Klein D, Rotarska-Jagiela A, Genc E, Sritharan S, Mohr H, Roux F, Han CE, Kaiser M et al (2014) Adolescent brain maturation and cortical folding: evidence for reductions in gyrification. *PLoS One* 9(1):e84914. <https://doi.org/10.1371/journal.pone.0084914>
 52. Desikan RS, Ségonne F, Fischl B, Quinn BT, Dickerson BC, Blacker D, Buckner RL, Dale AM et al (2006) An automated labeling system for subdividing the human cerebral cortex on MRI scans into gyral based regions of interest. *Neuroimage* 31(3):968–980. <https://doi.org/10.1016/j.neuroimage.2006.01.021>
 53. Hennig J, Weigel M, Scheffler K (2003) Multiecho sequences with variable refocusing flip angles: optimization of signal behavior using smooth transitions between pseudo steady states (TRAPS). *Magn Reson Med* 49(3):527–535. <https://doi.org/10.1002/mrm.10391>
 54. Chiarello C, Welcome SE, Halderman LK, Towler S, Julagay J, Otto R, Leonard CM (2009) A large-scale investigation of lateralization in cortical anatomy and word reading: are there sex differences? *Neuropsychology* 23(2):210–222. <https://doi.org/10.1037/a0014265>
 55. Ocklenburg S, Schlaffke L, Hugdahl K, Westerhausen R (2014) From structure to function in the lateralized brain: how structural properties of the arcuate and uncinate fasciculus are associated with dichotic listening performance. *Neurosci Lett* 580:32–36. <https://doi.org/10.1016/j.neulet.2014.07.044>
 56. Thomas C, Avram A, Pierpaoli C, Baker C (2015) Diffusion MRI properties of the human uncinate fasciculus correlate with the ability to learn visual associations. *Cortex* 72:65–78. <https://doi.org/10.1016/j.cortex.2015.01.023>
 57. Takao H, Hayashi N, Ohtomo K (2013) White matter microstructure asymmetry: effects of volume asymmetry on fractional anisotropy asymmetry. *Neuroscience* 231:1–12. <https://doi.org/10.1016/j.neuroscience.2012.11.038>
 58. Thiebaut de Schotten M, Ffytche DH, Bizzi A et al (2011) Atlasing location, asymmetry and inter-subject variability of white matter tracts in the human brain with MR diffusion tractography. *Neuroimage* 54(1):49–59. <https://doi.org/10.1016/j.neuroimage.2010.07.055>
 59. Henkelman RM, Stanisz GJ, Graham SJ (2001) Magnetization transfer in MRI: a review. *NMR Biomed* 14(2):57–64
 60. Zhang H, Schneider T, Wheeler-Kingshott CA, Alexander DC (2012) NODDI: practical in vivo neurite orientation dispersion and density imaging of the human brain. *Neuroimage* 61(4):1000–1016. <https://doi.org/10.1016/j.neuroimage.2012.03.072>
 61. Genç E, Fraenz C, Schlüter C, Friedrich P, Hossiep R, Voelkle MC, Ling JM, Güntürkün O et al (2018) Diffusion markers of dendritic density and arborization in gray matter predict differences in intelligence. *Nat Commun* 9(1):1905. <https://doi.org/10.1038/s41467-018-04268-8>
 62. Fjær S, Bø L, Myhr K-M, Torkildsen Ø, Wergeland S (2015) Magnetization transfer ratio does not correlate to myelin content in the brain in the MOG-EAE mouse model. *Neurochem Int* 83:84:28–40. <https://doi.org/10.1016/j.neuint.2015.02.006>
 63. Grussu F, Schneider T, Tur C, Yates RL, Tachrount M, İaşa A, Yiannakas MC, Newcombe J et al (2017) Neurite dispersion: a new marker of multiple sclerosis spinal cord pathology? *Ann Clin Transl Neurol* 4(9):663–679. <https://doi.org/10.1002/acn3.445>
 64. O'Muircheartaigh J, Dean DC, Dirks H, Waskiewicz N, Lehman K, Jerskey BA, Deoni SCL (2013) Interactions between white matter asymmetry and language during neurodevelopment. *J Neurosci* 33(41):16170–16177. <https://doi.org/10.1523/JNEUROSCI.1463-13.2013>
 65. Bartzokis G, Beckson M, Lu PH, Nuechterlein KH, Edwards N, Mintz J (2001) Age-related changes in frontal and temporal lobe volumes in men: a magnetic resonance imaging study. *Arch Gen Psychiatry* 58(5):461–465
 66. Sowell ER, Peterson BS, Thompson PM, Welcome SE, Henkenius AL, Toga AW (2003) Mapping cortical change across the human life span. *Nat Neurosci* 6(3):309–315. <https://doi.org/10.1038/mn1008>
 67. Chow JC, Yen Z, Ziesche SM, Brown CJ (2005) Silencing of the mammalian X chromosome. *Annu Rev Genomics Hum Genet* 6:69–92. <https://doi.org/10.1146/annurev.genom.6.080604.162350>
 68. Ocklenburg S, Ströckens F, Bless JJ, Hugdahl K, Westerhausen R, Manns M (2016) Investigating heritability of laterality and cognitive control in speech perception. *Brain Cogn* 109:34–39. <https://doi.org/10.1016/j.bandc.2016.09.003>
 69. Schmitz J, Kumsta R, Moser D, Güntürkün O, Ocklenburg S (2018) KIAA0319 promoter DNA methylation predicts dichotic listening performance in forced-attention conditions. *Behav Brain Res* 337:1–7. <https://doi.org/10.1016/j.bbr.2017.09.035>
 70. Ocklenburg S, Westerhausen R, Hirnstein M, Hugdahl K (2013) Auditory hallucinations and reduced language lateralization in schizophrenia: a meta-analysis of dichotic listening studies. *J Int Neuropsychol Soc* 19(4):410–418. <https://doi.org/10.1017/S1355617712001476>
 71. Ocklenburg S, Arning L, Hahn C, Gerding WM, Epplen JT, Güntürkün O, Beste C (2011) Variation in the NMDA receptor 2B subunit gene GRIN2B is associated with differential language lateralization. *Behav Brain Res* 225(1):284–289. <https://doi.org/10.1016/j.bbr.2011.07.042>
 72. Gould RM, Oakley T, Goldstone JV, Dugas JC, Brady ST, Gow A (2008) Myelin sheaths are formed with proteins that originated in vertebrate lineages. *Neuron Glia Biol* 4(2):137–152. <https://doi.org/10.1017/S1740925X09990238>
 73. Cartegni L, Chew SL, Krainer AR (2002) Listening to silence and understanding nonsense: exonic mutations that affect splicing. *Nat Rev Genet* 3(4):285–298. <https://doi.org/10.1038/nrg775>